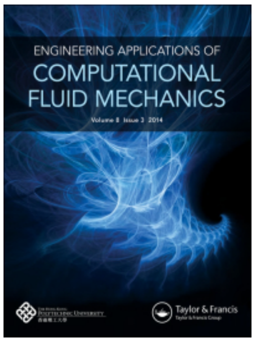

Taylor & Francis
Taylor & Francis Group

Engineering Applications of Computational Fluid Mechanics

ISSN: 1994-2060 (Print) 1997-003X (Online) Journal homepage: www.tandfonline.com/journals/tcfm20

Development and validation of a CFD-based model for simulating rotating drum separators

Theodoros Dimas, Arne Eggers, Jef R. Peeters & Maarten Vanierschot

To cite this article: Theodoros Dimas, Arne Eggers, Jef R. Peeters & Maarten Vanierschot (2024) Development and validation of a CFD-based model for simulating rotating drum separators, Engineering Applications of Computational Fluid Mechanics, 18:1, 2368606, DOI: 10.1080/19942060.2024.2368606

To link to this article: https://doi.org/10.1080/19942060.2024.2368606

Published online: 06 Jul 2024.

ENGINEERING APPLICATIONS OF COMPUTATIONAL FLUID MECHANICS
2024, VOL. 18, NO. 1, 2368606
https://doi.org/10.1080/19942060.2024.2368606

Taylor & Francis
Taylor & Francis Group

OPEN ACCESS Check for updates

Development and validation of a CFD-based model for simulating rotating drum separators

Theodoros Dimas[a], Arne Eggers[a], Jef R. Peeters[a,b] and Maarten Vanierschot[a,c]

[a]KU Leuven, Department of Mechanical Engineering, Group T campus Leuven, Leuven, Belgium; [b] Flanders Make @ KU Leuven, Leuven, Belgium; [c]Material Science, Innovation and Modelling (MaSIM), North-West University, Mmabatho, South Africa

ABSTRACT
Within the context of the European Green Deal, recycling rates of plastics and metals are targeted to increase which will subsequently increase the requirements for high-quality recycled plastics and metals. The decisive step to achieve this high-quality recyclate lies in the sorting of the materials before their recycling. Density separation sorts materials based on their density difference from a liquid's density and is the most widely used separation technique in the industry because of its high cost-effectiveness. However, experimentally optimising a density separator would require a large amount of time and investment due to its large dimensions and the complex physical phenomena involved. Hence, the scope of this study is to develop a Computational Fluid Dynamics (CFD) model to investigate the fluid flow and trajectories of plastic particles in a density-separation-based rotating drum. This novel strategy and CFD model offer a tool capable of predicting the separation efficiency with an absolute error of 1–5%, depending on the polymer type, while reducing the computational time by a factor of 9. Moreover, the influence of air bubble attachments to the injected particles in the drum is observed and the inclusion of inter-particle collisions on the accuracy of the model is assessed.

ARTICLE HISTORY
Received 12 March 2024
Accepted 8 June 2024

KEYWORDS
Rotating drums; density separation modelling; computational fluid dynamics; discrete phase model

1. Introduction

The European Strategy for plastics was formulated within the context of the European Green Deal, which arises from the European Union's commitment to becoming climate-neutral by 2050. Through the above-mentioned strategy, the European Union has introduced policies and directives for the transition to a more sustainable use of plastics to achieve the following goals by 2030: recycling or reusing all packaging waste, recycling half of all plastic waste in Europe, becoming a leader in innovative sorting and recycling equipment, and phasing out the production of chemical additives that hinder recycling (European Commission, 2018). However, the potential for plastic recycling remains limited, with only 35% of plastic waste being sent for recycling and only 45% of recyclates being used in new products (PlasticsEurope, 2022). The main reasons for this lie in the fact that (1) recycled plastics are of low quality, making them inadequate to replace virgin plastics and (2) inconsistencies during the recycling process lead to losses of large amounts of plastic during sorting (European Commission, 2022). To achieve high-quality recycled plastics, high purity on the polymer level is needed during the sorting process due to the immiscibility of polymers at a molecular level. For instance, for polyethylene (PE) and polypropylene (PP), which are some of the most common plastics, their purity should be above 97% when separated so that they can be compared to virgin PP and PE after recycling (Bakker et al., 2009). Hence, sorting is the decisive step that can contribute to increasing the quality of the recyclates and preserving the amount of plastic waste heading to recycling as close to the input as possible.

The state-of-the-art sorting method in mechanical recycling is density separation due to its high processing capacity and cost-effectiveness (Froelich et al., 2007; Gent et al., 2009). Density separation is based on the Archimedes principle where the plastics have a density above the separating medium sink and the plastics have a density lower than the separating medium float. The combination of a rotating drum with flotation, which is a process of changing the wettability of the plastic surfaces, achieved high purities in separating polyethylene terephthalate (PET) from PP and PE (Dodbiba et al., 2002). Additionally, various other density-based separation methods exist in the literature such as magnetic density separation, which combines the sink-float separation principle with a magnet to create a magnetic field that induces a pressure gradient vertically in the tank

CONTACT Maarten Vanierschot maarten.vanierschot@kuleuven.be Celestijnenlaan 300, B-3001 Leuven, Belgium

hence affecting the apparent density of the fluid (Serranti et al., 2015; Tierean et al., 2012). This method's main benefit is its capability to sort multiple polymer types in a single step. However, the high costs mainly related to reclaiming, washing and diluting the magnetic fluid still make this process expensive, although it has been applied in some recycling companies, especially in the Netherlands (Bakker et al., 2009). Moreover, there is jigging separation, which combines the Archimedes principle with pulsations on the flow, exhibited great potential in achieving high purities (Hori et al., 2009). However, the above-mentioned technique has not been applied on an industrial scale.

The main reasons that make rotating drums state-of-the-art in material separation are their ability to process pieces of 6–160 mm length scale and their low operational costs (Rousseau & Melin, 1989). Furthermore, they are known to be effective for material mixtures of strongly differing densities such as automotive scrap (Gaustad et al., 2012). The objects with a higher density than the medium (heavies) sink and are being swept by the lifter which are rotating along with the drum and the objects with a lower density than the medium (lights) follow the fluid stream of the free surface since the drum is inclined. Modern rotating drums have curtains to prevent lights from entering the sink lifter pick-up zone on the medium surface. If heavies leave the drum through the float outlet or lights through the sink outlet, they get misplaced, reducing the purity of the separated material stream and yield of the process. The reason for misplacement depends on the field of application. In plastics recycling, polymers are mainly hydrophobic and thus the probability of air-bubbles attached to the plastic objects is increased. Hence, because of the small difference between the medium and separation object density, the bubbles attached to the separation objects influence their effective density significantly and may introduce misplacement.

Due to the fact that rotating drums, as well as density separation in general, involve complex phenomena such as turbulence, particle hydrodynamics, free surface interaction with moving geometries and bubbles generation and attachment on the particles, first-order models (Baguley & Napier-Munn, 1996) are not sufficient to optimize the separation efficiency up to the required standards. Therefore, to examine the fluid flow inside the drum and the interaction between the flow and particles, CFD models need to be developed for modelling rotating drums and other density separation techniques. CFD models have been developed recently in order to optimize separation processes in various industries, such as coal separation (Xia & Peng, 2007), water and oil separation (Yayla et al., 2017), colloidal particles separation from water (Halfi et al., 2020), separation of active components of lithium-ion batteries (Pang et al., 2022) and threshing of rice (*J.* Yuan et al., 2020). In the realm of plastics and metals sorting, several studies have implemented CFD modelling for different applications. This includes hydro-cyclones (*H.* Yuan et al., 2015) and magnetic density separation of plastics (Tajfirooz et al., 2021), dense medium drums for metal separation (Eggers et al., 2019) and separation of polyvinyl chloride and copper from cables by mechanical agitation (Lu et al., 2019).

Studies that have implemented CFD to investigate the flow inside a rotating drum for plastics separation are more limited. The first study to model a lab-scale rotating drum, which separates plastics, followed a Lagrangian-Lagrangian (LL) approach in the sense of modelling both the fluid flow and the granular phase as particles (Markauskas et al., 2018). Nevertheless, the model was not validated by experimental results and the computational efficiency was not mentioned, making it difficult to use that model in order to assess the suitability of a rotating drum for plastics separation. In general, besides LL two other approaches are more widely used when modelling the interaction of a dispersed solid phase within a liquid. The first is Eulerian- Eulerian (EE) which treats both liquid phase and dispersed phase as a continuous medium and has been implemented in several CFD studies to investigate the trajectory of the solid phase inside a rotating drum, although not for material separation processes (Santos et al., 2013), (Zhu et al., 2020), (Rong et al., 2020). The second approach is Eulerian - Langrangian (EL) which treats the carrier phase as a continuous medium and the dispersed solid phase as particles, tracking every particle's trajectory based on the hydrodynamic forces acting on it and provides more accurate particle-scale information such as particles trajectories (Nascimento et al., 2022),(Panchal & Menon, 2021) and is more grid-independent than the EE approach (Adnan et al., 2021). In the field of plastics and metal separation for recycling, capturing accurately the trajectories of the dispersed solid phase that includes particles of different sizes and densities is essential.

In this study, a Computational Fluid Dynamics (CFD)-based model is developed in order to model the flow inside a rotating drum and calculate the trajectories of plastic particles that are injected into the drum. The approach implemented in this study is the Euler – Lagrange framework in which the Reynolds Averaged Navier Stokes (RANS) equations are employed to model the fluid flow and the Discrete Phase Model (DPM) including turbulent dispersion is employed to track the plastics inside the drum. Furthermore, this study includes implementation of a new simulation strategy within the EL approach to track the dispersed solid

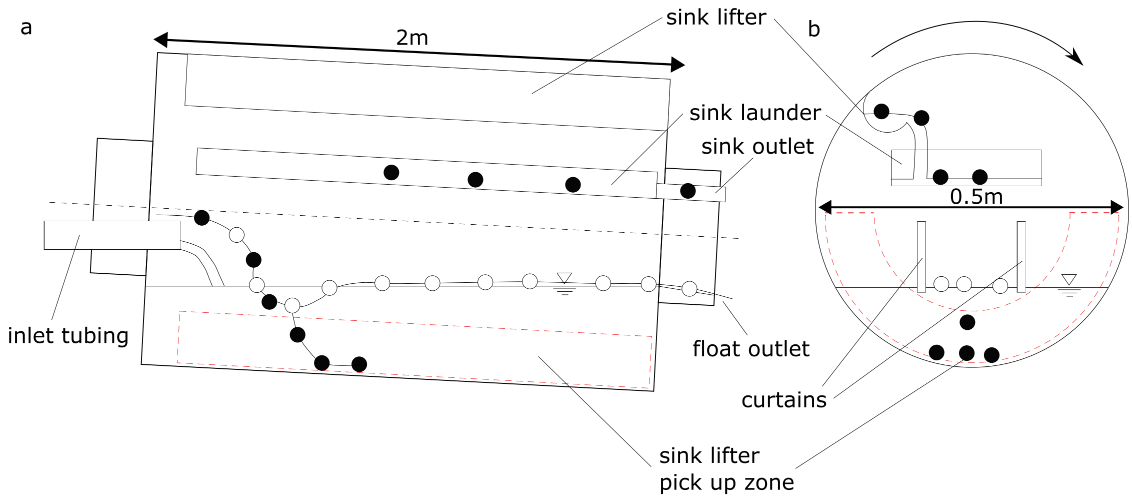

Figure 1. Two views of the experimental setup with the trajectories of heavy and light objects (Eggers, 2020).

objects in the moving rotating drum by separating the fluid flow simulation and particle tracking using the periodic flow regime in the drum. This approach decreases the simulation time by a factor of 9, allowing simulations of various particle densities within reasonable computational times to derive separation curves of the drum. Moreover, this study includes the implementation of a Discrete Phase Model - Discrete Element Model (DPM-DEM), which takes into account the particle collisions in order to assess their influence on the predicted separation efficiency. The predicted by the CFD model separation efficiencies are compared to experimentally derived ones to validate the model and in this comparison the influence of bubbles attachments to the separation efficiency is accentuated. In conclusion, the followed methodology of this study can be implemented to model a rotating drum in a wide variety of industries (such as mining, separation, water treatment etc.) in order to optimize their working parameters in an affordably – for industry and research- simulation time. An additional insight from this study is that rotating drums are not an ideal solution for plastics separation, due to the large misplacements created by the high turbulent flow inside a rotating drum.

2. Materials and methods

2.1. Experimental setup and materials

Figure 1 depicts the experimental setup utilized in this study (Eggers, 2020). A laboratory-scale rotating drum is employed, which is slightly inclined to ensure a consistent fluid outflow that facilitates the movement of floating plastics to their corresponding output, which is called hereafter float outlet. Additionally, sinking plastics are collected by a lifter, and at the top of the drum, they are allowed to fall upon a baffle, which directs them to their corresponding output. The medium that is utilized in the experiments is water, which is pumped into the drum from a buffer tank. Materials are fed into the drum near the inlet while the drum and the lifter rotate at an angular velocity of $\omega = 0.508\, rad/s$. The materials to be separated are plastic granules whose shape is cylindrical with a diameter and length ranging from $3\,mm$ to $4\,mm$. As the aspect ratio of the particles is about 1, the shape factor is in the order of unity and as such, the particles were assumed to have a spherical shape in the CFD model. The validity of this approach is demonstrated in the work of (Dimas et al., 2024). The specific characteristics of the particles are listed in Table 1. Furthermore, two different types of polymers with similar densities one being hydrophobic and the other one hydrophilic have been selected to evaluate the influence of the air-bubbles, which are formed during the impact of the plastics and the fluid's free surface, on the separation efficiency. The separation efficiency is calculated as

$$Sep_{sink} = \frac{m_{sink}}{m_{sink} + m_{fl}}, \tag{1}$$

where m_{sink} and m_{fl} is the mass of the particles collected by the lifter or exiting the float outlet respectively. Sep_{sink}

Table 1. Polymer type, density, size and characteristics of the materials.

	PP[a]	HDPE[b]	PS[c]	ABS[d]	PC/ABS[e]
$\rho\,[kg/m^3]$	900	946	1040	1040	1150
$d[m]$	0.003	0.004	0.003	0.003	0.003
specific characteristics	–	–	hydrophobic	hydrophilic	–

[a]Polypropylene. [b]High Density Polyethylene. [c] Polystyrene. [d]Acrylonitrile butadiene styrene. [e]Polycarbonate/Acrylonitrile butadiene styrene.

is the separation efficiency based on the particles collected by the lifter and is calculated for the material types that would normally result to that exit (heavies). Consequently, to calculate the separation efficiency for the particle types whose density is lower than the liquid's, Sep_{fl} is calculated from the following equation:

$$Sep_{fl} = \frac{m_{fl}}{m_{sink} + m_{fl}}. \tag{2}$$

2.2. Numerical modelling

In this study, the Euler–Lagrange (EL) approach is followed, which considers the fluid as a continuous phase and the solid particles as discrete entities. Specifically, a one-way coupling EL method is implemented, where the influence of the fluid flow on the particles is accounted for, but not vice versa. The governing equations for the fluid flow and the equations of motion for the particles are presented in the following subsequent sections.

2.2.1. Fluid flow modelling

For simulating the fluid flow, the unsteady incompressible RANS equations in their conservation form are discretized using the Finite Volume method implemented in Ansys Fluent (ANSYS Inc., 2020):

$$\frac{\partial(\rho \bar{u}_i)}{\partial x_i} = 0, \tag{3}$$

$$\frac{\partial(\rho \bar{u}_i)}{\partial t} + \frac{\partial(\rho \bar{u}_i \bar{u}_j)}{\partial x_j} = -\frac{\partial \bar{p}}{\partial x_i} + \frac{\partial \bar{T}_{ij}}{\partial x_j} - \frac{\partial(\overline{u_i' u_j'})}{\partial x_j} + g_i, \tag{4}$$

where $\bar{u}_i$ is the Reynolds averaged velocity, x_j the spatial coordinate, t the time, ρ the density, $\bar{p}$ the Reynolds averaged pressure, $\bar{T}ij$ the mean viscous stress tensor, $\overline{u_i' u_j'}$ the Reynolds stress tensor and g_i the gravitational acceleration. Moreover, the turbulent fluctuations of the fluid stream in the rotating drum are modelled using the k-ω SST turbulence model as proposed by Menter (1994), which incorporates two blending functions dependent on the wall distance to switch between k-ω and k-ϵ models and prevent overestimation of the shear stress near the wall. Therefore, the aforementioned model is robust in a wide range of Reynolds numbers and wall resolutions, which is an important aspect to consider for industrial applications. Furthermore, the fluid flow in the rotating drum comprises of two fluids: a liquid, which in our case is water and a gas, which is air. A distinct boundary of varying density, referred to as the free surface, separates these two fluids and moves unrestrictedly. The explicit Volume of Fluid (VOF) model, is employed in this study to simulate the free surface motion (Hirt & Nichols, 1981). The fundamental principle of VOF is the non-interpenetration of the two fluids and it solves a transport equation of a scalar function ϕ which indicates the volume fraction of every fluid per computational cell. The summation of ϕ for all phases over every cell in the computational domain should be equal to unity. In the present case, $\phi = 1$ indicates the presence of water, $\phi = 0$ indicates the presence of air, and $0 < \phi < 1$ indicates the free surface. Eventually, the local properties such as density and dynamic viscosity at every cell are volume averaged based on the volume fraction of the phases:

$$\rho = \phi \rho_{med} + (1 - \phi)\rho_{air}, \tag{5}$$

$$\mu = \phi \mu_{med} + (1 - \phi)\mu_{air}. \tag{6}$$

2.2.2. Plastic particles simulation

The Discrete Phase Model (DPM) is utilized to model the behaviour of the dispersed solid particles as shown in Figure 1. DPM applies Newton's second law to determine the position of each particle by considering the drag, buoyancy and gravitational forces at each time step. DPM assumes negligible change in the volume fraction of the continuous phase, as it is not displaced by the dispersed phase and thus, DPM is particularly suitable for accurately representing dilute particle flows, where the volume fraction of particles is less than 10% of the total volume fraction. As stated earlier, the simulation strategy employed in this study follows a one-way coupling approach, wherein the equations governing the fluid flow are solved independently of the particle equations. Consequently, the forces acting on the particles are only updated at each iteration when the flow properties are updated,

$$m\frac{d(\overrightarrow{u_p})}{dt} = \overrightarrow{F_d} + \overrightarrow{F_b} + \overrightarrow{F_g}, \tag{7}$$

where $\overrightarrow{u_p}$ is the particle's velocity and $\overrightarrow{F_d}$ is the drag, $\overrightarrow{F_b}$ the buoyancy force and $\overrightarrow{F_g}$ the gravitational force respectively. In this study particles are assumed to be spherical and thus the summation of the buoyancy and gravity forces can be written as:

$$\overrightarrow{F_b} + \overrightarrow{F_g} = \frac{4}{3}(\rho_p - \rho_f) r^3 \vec{g} \pi, \tag{8}$$

where ρ_p is the particle's density, ρ_f is the fluid's density and r is the particle's radius. The drag force is calculated through the following formula:

$$\overrightarrow{F_d} = \frac{1}{2}\rho_f C_d(\vec{v}_{rel})|\vec{v}_{rel}|A, \tag{9}$$

where $\vec{v}_{rel}$ is the vector of the relative velocity between the fluid and the particle, A is the area of the spherical particle and C_d is the coefficient of drag. The drag coefficient is determined through various empirical drag laws. These laws, which are formulated based on the shape of the particle, the properties of the fluid, and the Reynolds number (Re), have been developed to accurately predict the drag force experienced by an object in a given flow regime. The spherical drag law is utilized to compute the drag coefficient:

$$C_d = a_1 + \frac{a_2}{Re_p} + \frac{a_3}{Re_p^2}. \tag{10}$$

The coefficients a_1, a_2 and a_3 have been found by Morsi and Alexander (1972) per different particle Reynolds numbers Re_p, defined as:

$$Re_p = \frac{\rho_f \vec{v}_{rel} d_p}{\mu}, \tag{11}$$

where d_p is the particle diameter and μ the dynamic viscosity.

2.2.3. Turbulent dispersion of particles

To include the influence of turbulence on the particles' trajectories, a fluctuation term is introduced in their motion through the discrete walk or eddy interaction model, as was introduced by (Gosman & Loannides, 1983). This model assumes isotropic turbulence and incorporates a stochastically varying velocity term in the local flow velocity as:

$$\vec{u}_{new} = \vec{u}_{local} + \vec{u}', \tag{12}$$

where $\vec{u}_{new}$ is the local flow velocity vector after having incorporated the stochastic term $\overrightarrow{u'}$, which is calculated using a Gaussian distribution function and the turbulent kinetic energy,

$$\overrightarrow{u'} = \vec{\sigma} \cdot \sqrt{\frac{2}{3}k}, \tag{13}$$

where σ is a function which generates random numbers normally distributed and k is the turbulent kinetic energy which for isotropic turbulence is $k = 3/2(u'^2) = 3/2(v'^2) = 3/2(w'^2)$ (u', v' and w' are the local RMS values of the fluctuating velocity component). The characteristic eddy lifetime t_e is used to define the frequency with which the stochastic velocity term will be updated in equation 12:

$$t_e = \frac{3.33}{\omega}, \tag{14}$$

where ω is the turbulence dissipation rate.

Table 2. Predicted separation efficiency for PP and PS for three different coefficients of restitution.

	η_1	η_2	η_3
PP	10%	11%	11%
PS	96%	96%	96%

2.2.4. Particle collisions

The DPM model has the potential to be integrated with the Discrete Element Method (DEM) to take into account the collisions between particles mutually and between particles and walls. Therefore, an additional term for the collision force on the particle is added in the DPM as can be seen in Equation (15):

$$m\frac{d(\overrightarrow{u_p})}{dt} = \vec{F}_d + \vec{F}_b + \vec{F}_g + \overrightarrow{F_{col}}. \tag{15}$$

DEM is making use of a collision force law which calculates the above-mentioned force from the overlap between particles or between particles and a boundary (Cundall & Strack, 1979). The collision force law utilized in this study is the linear spring – dashpot model (LSD), which calculates the collision force on the particle from Equation (16):

$$\overrightarrow{F_{col}} = (\kappa\delta + \gamma\,(\overrightarrow{v_{12}}\overrightarrow{e_{12}}))\overrightarrow{e_{12}}, \tag{16}$$

where κ is the spring constant, δ is the overlap between the particles, γ is the damping coefficient, $\overrightarrow{v_{12}}$ is the relative velocity between the two particles and $\overrightarrow{e_{12}}$ is the unit vector on the direction of the two particles. Both particle-particle and particle-wall collisions are assumed to have the same model parameters (Dimas et al., 2024). The value of the spring constant is estimated by making use of Equation (17), so as to ensure that the overlap between two particles doesn't exceed 0.1% of the particle diameter (Hilton & Cleary, 2014).

$$\kappa = \frac{\pi v^2}{3\delta^2} d_p, \tag{17}$$

where v is the relative velocity between the particles and d_p is the particle diameter. Moreover, a sensitivity study took place on the influence of coefficient of restitution on the predicted separation efficiency for light particles (PP) and for heavy particles (PS). As shown in Table 2, three coefficients of restitution $\eta_1 = 0.1$, $\eta_2 = 0.5$ and $\eta_3 = 0.9$ were compared, showing that the predicted separation efficiency remains unaffected. The coefficient of restitution utilized in this study is set to 0.5 for all particles densities.

2.2.5. Case setup

The boundary conditions of the rotating drum are illustrated in Figure 2. Moreover, the pressure at the outlet is

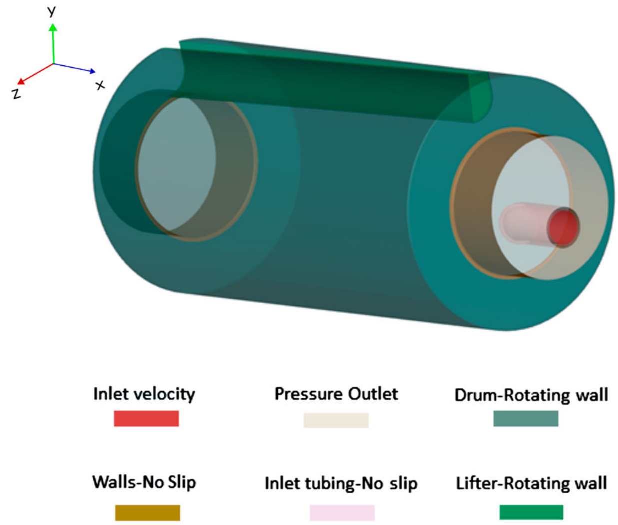

Figure 2. Boundary conditions of the rotating drum.

Table 3. Setup conditions for the flow and the particles.

	V_{inlet} (m/s)[a]	ω_{wall} (rad/s)[b]	$\dot{m}_p$(kg/s)[c]	t_i (s)[d]
values	0.114	0.508	0.127	1

[a]Velocity of the inlet. [b]Angular velocity of drum walls. [c] Mass flow rate of particles. [d]Injection duration.

set equal to atmospheric pressure, and the no-slip boundary condition at the walls imposes zero relative velocity between fluid and wall and thus the fluid velocity is equal to the wall velocity there. The velocity of the fluid at the inlet and the angular velocity of the walls are indicated in Table 3. Concerning the initial conditions of the particles, in every case a single plastic type was injected with three injections taking place in total, each with a mass flow rate of 0.127 kg/s (Table 3), resulting in between 22 and 29 thousand particles being injected. The boundary conditions for the discrete solid phase include reflection of the particles at the walls, except for the lifter and the float outlet, where the particles are not being tracked upon their contact on these surfaces.

The computational mesh used in this study has undergone a grid independence study of which the results are detailed in the study of Eggers (2020). The sizes of the three computational grids utilized are depicted in Table 4, showing values for the maximum velocity magnitude and maximum x-velocity component of the medium phase in every grid, together with separation efficiencies for particles close to the density of water. As the differences in separation efficiencies are within 1% compared to the fine grid, and to decrease the computational cost, the medium mesh is utilized in this study. The average maximum included angle which is a measure of skewness is 96.5° and the cells have an average volume ratio of 1.2. The Y + values of the mesh vary between 16 and 80, which

Table 4. Computational grids size and grid independence study (Eggers (2020)).

	coarse	medium	fine
cell count	553.853	1.535.506	4.236.097
max. x-velocity component (m/s)	1.57	1.63	1.62
max. velocity magnitude (m/s)	1.86	1.99	2.1
separation efficiency 980 kg/m^3 particles	78%	83%	84%
separation efficiency 990 kg/m^3 particles	92%	87%	87%

is within an applicable range of the chosen turbulence model.

The sliding mesh approach was adopted to model the motion of the lifter that collects sinking particles. To implement this approach, the following methodology was employed. Two separate meshes were created: one consisting of the inlet and outlet, which is a stationary mesh as depicted in Figure 3(a) and one consisting of the lifter and the outer part of the drum, which is a rotating mesh as illustrated in Figure 3(b). At the region where both meshes have adjacent cells, an interface zone is created. At this interface zone, the fluid flow properties are interpolated from one mesh to the other to maintain continuity across the interface. In Figures 3(c & d), the position of the lifter at different time steps is illustrated to make their motion more lucid. The rotating cell zone consists of only hexahedral cells, while the stationary cell zone consists of mainly hexahedral cells along with tetrahedral in the region of the inlet as it can be seen in Figure 3(e).

2.3. *Simulation strategy*

The strategy employed to model the trajectory of plastic objects inside the drum takes advantage of the periodic flow developed inside the rotating drum and was tested and validated with the study of Greifzu et al. (2016) before implemented in this study. As depicted in Figure 4, the fluid flow inside the rotating drum evolves into a periodic regime. During the third period, the flow field data, which includes the pressure field, velocity field, turbulent kinetic energy, specific dissipation rate, and volume fraction of the two phases (air and water), is exported every dt. Henceforth, there is no need to solve the fluid flow equations along with the particle equations as a periodic regime was reached by the flow and hence, only the DPM equations are being solved, as is depicted in Figure 5. At the first time-step $\mathbf{t}_0$ of the periodic regime, the flow field and the mesh are imported, the particles equations are solved and as a result particles positions are updated. Subsequently, the non-stationary cell zone is rotated for one-time increment (dt). Upon reaching the next time step, the fluid flow at that step is imported, and the same

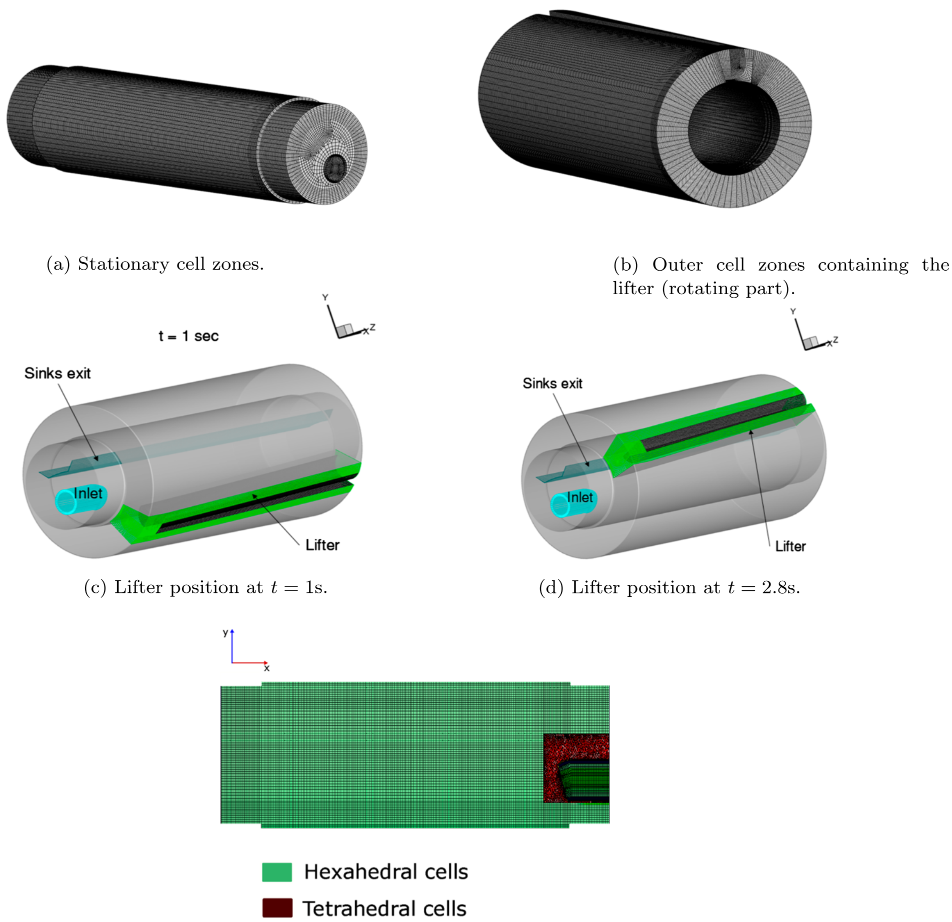

(a) Stationary cell zones.

(b) Outer cell zones containing the lifter (rotating part).

(c) Lifter position at $t = 1$s.

(d) Lifter position at $t = 2.8$s.

(e) Cell type at a cross section of the stationary cell zone.

Figure 3. Cell zones and illustration of the moving mesh.

process is repeated. Finally, it should be noted that the integration time of Equation (7) is set equal to the flow time step.

2.4. Correction of the sloshing effect

Figure 6(a) illustrates that the converged periodic regime is not entirely periodic meaning that the last time-step of the period is not equal to the first time-step of the next period and thus creating a non continuous velocity field when applying the above-mentioned methodology. This deviation takes place mainly due to two factors: (a) the interaction between the lifter and the free surface and (b) the fact that water is falling from the lifter during its rotation. Therefore, to explicitly impose continuity of the flow velocity between the last time steps and the first time steps, the following technique is applied. The velocity field at the last and first time-step of the period is averaged and afterward is assigned at both aforementioned time-steps. Moreover, over the last 15 time steps of the period, the newly averaged flow field of the succeeding time-step is averaged with the flow field at the specific time-step to ensure a smoother velocity field. Accordingly, the velocity field for the first 10 time steps is also smoothed. The three velocity components at a specific cell of the stationary cell zone are depicted in Figures 6(a, b and c) before and after applying the above-mentioned correction.

3. Results

3.1. Velocity field in the separator

Given that the lifter initiates its movement from the top at the beginning of the period, Figure 7 illustrates the x-velocity component on the separator's free surface at four key points in time: $T/4$ seconds before the lifter reaching the drum's bottom, upon reaching the bottom position, $T/4$ seconds after that and when reaching at the top position of the drum after one period of rotation. The free-surface is visualized by iso-surfaces of ϕ being equal to 0.5. Along the drum's lengthwise direction, three distinct flow patterns emerge, each assigned to different regions. In region b, positioned in the middle of the drum, a high-velocity component in the lengthwise

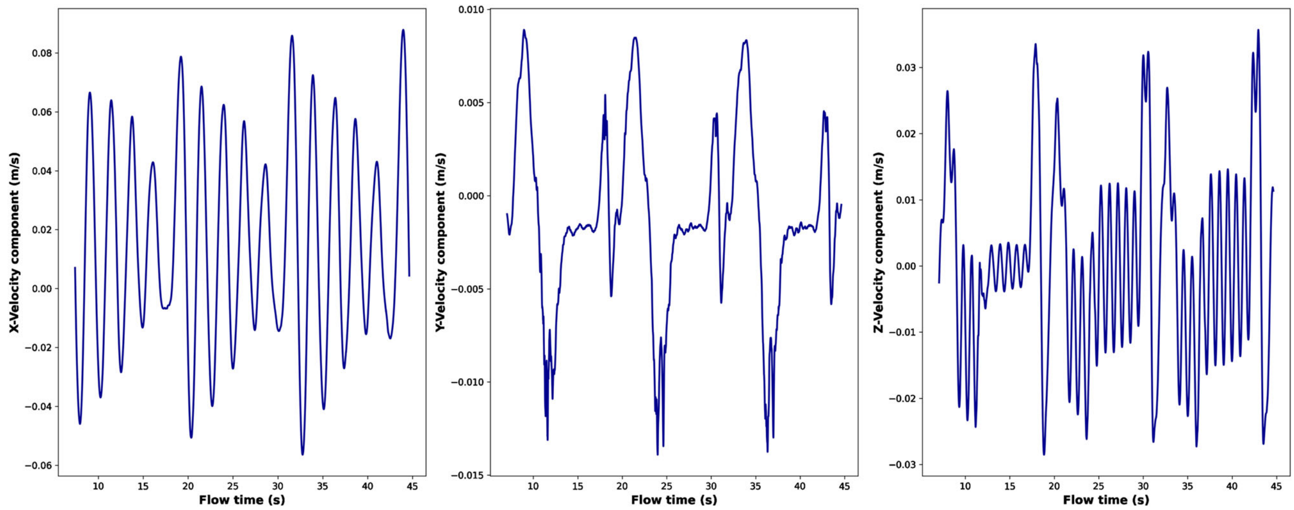

Figure 4. Periodic regime reached for the three components of the volume averaged velocity of the medium phase.

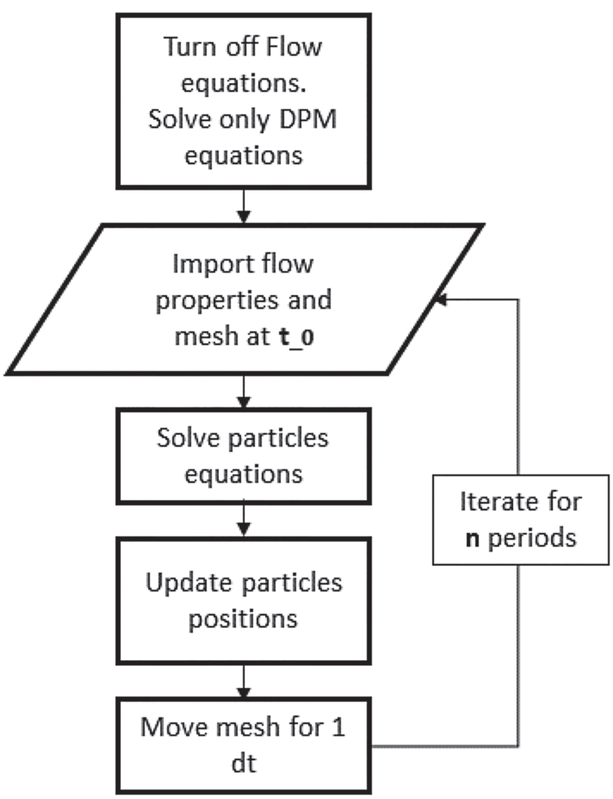

Figure 5. Strategy for simulating the trajectories of the plastics objects in the drum.

direction is evident, generated by the inlet tube in this region. Further downstream in this area, a recirculation zone appears both before and after the lifter submerges into the water. This recirculation area exists in region b during the whole period. Another notable flow pattern on the free surface involves a motion perpendicular to the lengthwise direction, which is occurring in region c. This pattern is attributed to the counterclockwise rotation of the drum, causing the lifter to drag water as it submerges (on the side of region a) and emerges (on the side of region c), thereby inducing a similar motion in the fluid occupying the space displaced by the lifter. This motion can also be seen in Figure 8, which illustrates the contour of the z-velocity component along with the streamlines at a slice normal to the x axis in the middle of the drum. Another insight from Figure 8 is that when the lifter is at the bottom, a vertical motion is induced in the fluid which can drag floating particles that have been recently injected and are located slightly lower than the free-surface, entrapping them in recirculation zones behind the lifter. It can thus be concluded that the optimal drop-off location would be in region b, and injection should occur only when the lifter has passed the bottom of the drum or is above the medium's surface to ensure that the floating particles are not dragged by the flow field towards the bottom but move towards the float outlet.

Figure 9 illustrates the velocity magnitude and streamlines of the flow field at a cross-section normal to the z-axis in the middle of the drum, captured at $1/4T$ seconds and $3/4T$ seconds. Notably, it is observed that before the lifter is submerged into the water, it is relatively safe to release particles in proximity to the inlet. However, this location does not persist after the lifter has emerged from the water. In the latter case, if the drop off location is close to the inlet, there is a high probability of the particles being trapped in a recirculation zone situated to the left of the water inlet location.

3.2. Particles trajectories and distribution

3.2.1. Trajectories of light particles, baffle-curtains implementation and injection location influence

To maintain readability and avoid text density, only the trajectories of PP particles are presented in Figure 10 as

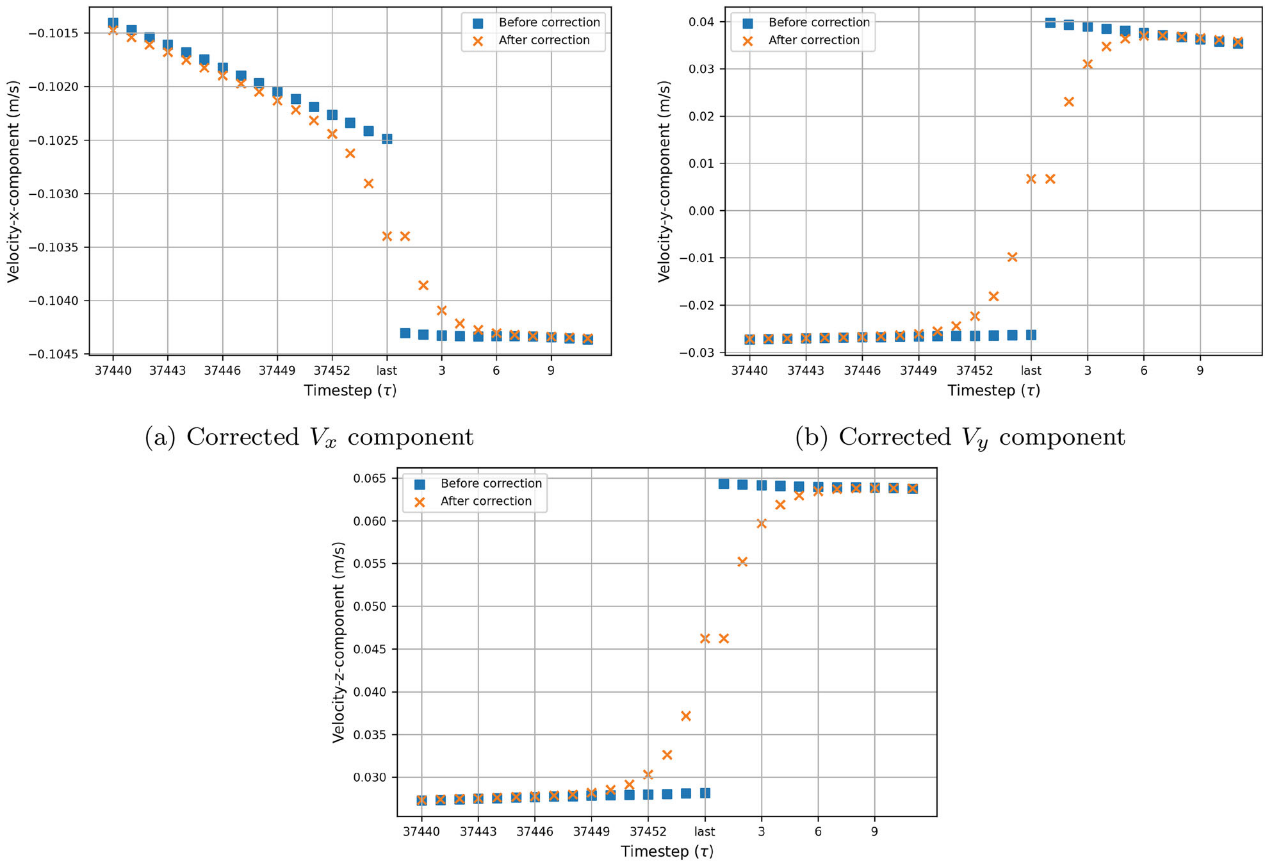

(a) Corrected V_x component

(b) Corrected V_y component

(c) Corrected V_z component

Figure 6. Corrected velocity components.

those of other particles are very similar. The time-frame is chosen from the start of the second period to the end of the third one and the particles have been labelled with a different colour to distinguish between their injection times. Moreover, the recirculation zones detected in the flow field of the free surface can also be seen in the particles trajectories and have been marked with a black ring.

Table 5 indicates that the predicted by model separation efficiency of PP particles is 10–13% and of PE particles 11–12% which deviate 1–4% from the experimentally derived ones. With respect to the model's accuracy, the deviation is mainly attributed to the assumption of having spherical particles while in reality the particles were cylindrical. With regards to the process, only 10–13% of PP and 8–11% of PE particles end up at the float outlet indicating a very low efficiency in sorting polymers with a lower density than the medium's. However, this low efficiency can be explained by the absence of baffles on the free surface which could prevent the floating particles from floating towards the regions of the lifter and thus possibly being swept by it. Figure 11(a) illustrates the cumulative mass of PS and PP particles that are swept by

Table 5. Separation efficiencies of the two simulated cases and the experiment.

Polymer type	$Sep_{1stcase}$ (%)[a]	$Sep_{2ndcase}$ (%)[b]	$Sep_{exp.}$ (%)[c]
PP	10	13	–
PE	11	12	8 ± 2
PS	96	96	54 ± 6
ABS	96	96	77 ± 2
PC	99	99	94 ± 2

[a]With particle collisions. [b]Without particle collisions. [c]Experimental results.

the lifter across the width of the drum. Considering that the lifter's width is 0.13 m, it can be deduced that the lack of curtains on the free surface contributes to roughly 82% of the PP particles reaching the sink exit. Hence, in case baffles are placed 5 cm from the centre of the drum to prevent the floating particle trajectories towards the lifter regions, as depicted in Figure 11(b), the misplacement of floating particles at the lifter will be reduced from 89% to 8%.

On the other hand, PS particles, which are heavier than water, are swept across the entire width of the separator by the lifter. Furthermore, Figure 11(a) reveals that 8% of PP (Polypropylene) particles are swept by the

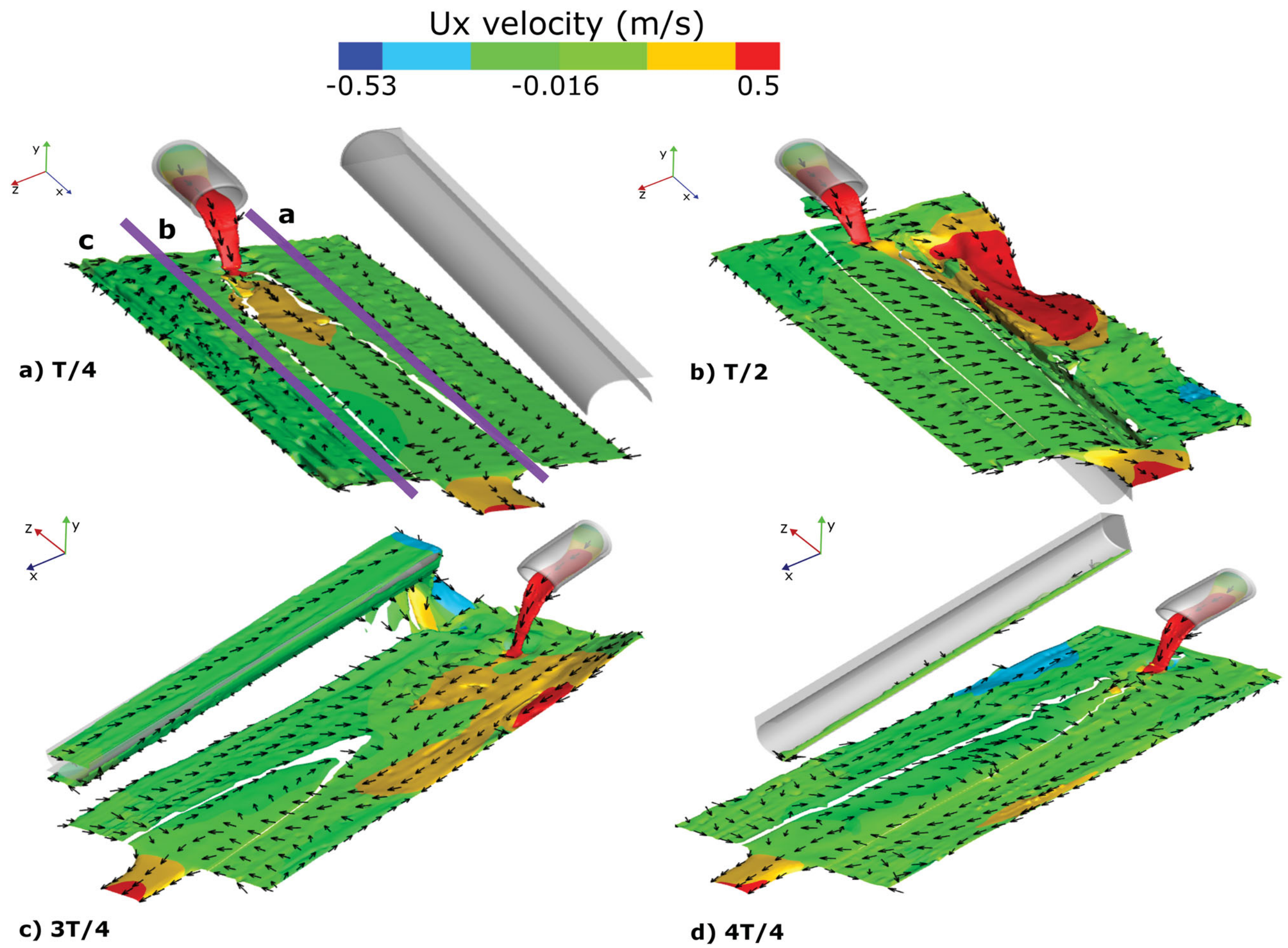

Figure 7. X-velocity component on the free surface at four different time instances. The view is rotated to reveal the details on the lifter.

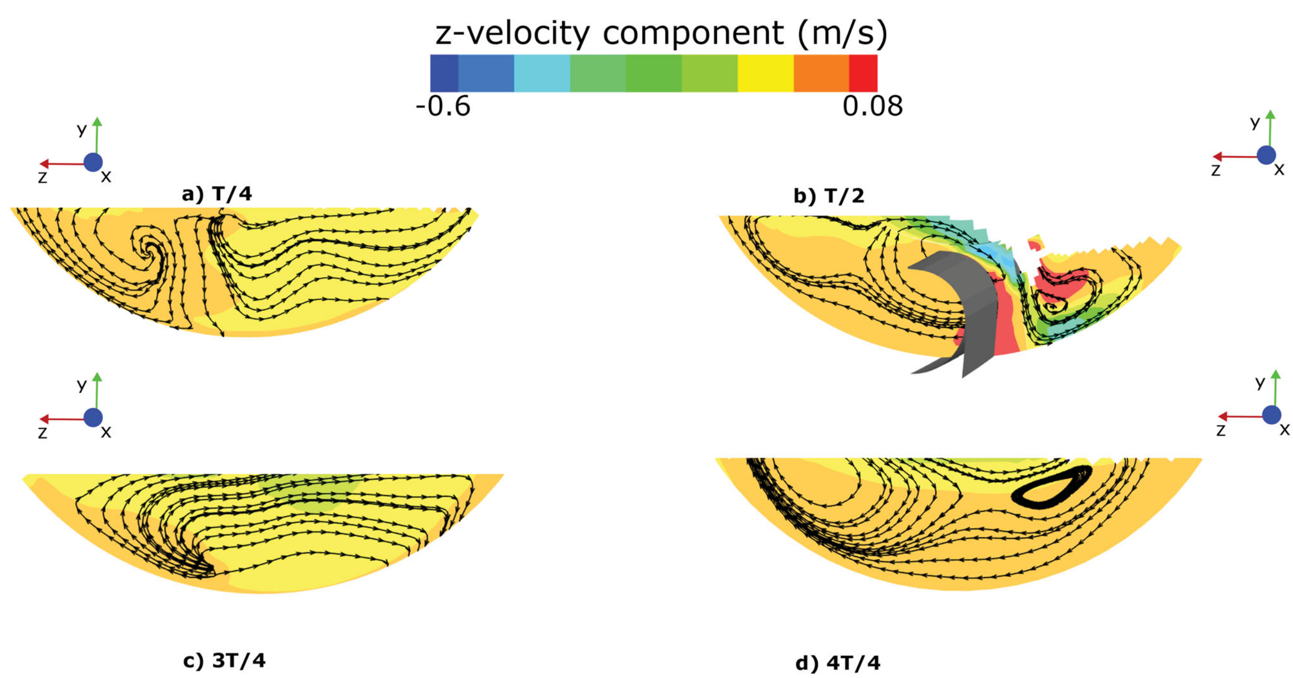

Figure 8. Z-velocity component at the middle of the separator at four different time instances.

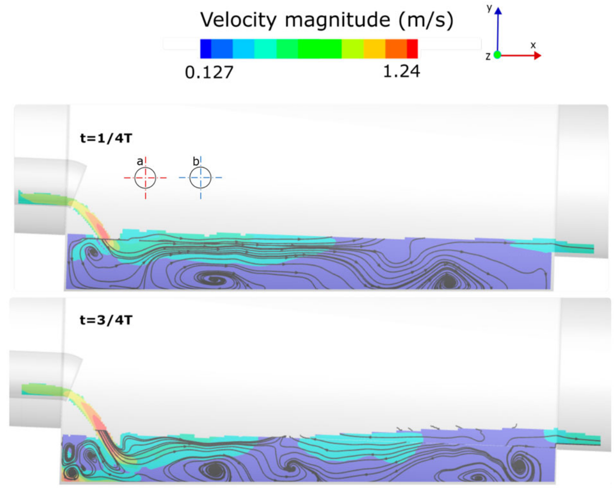

Figure 9. Velocity magnitude at the middle of the separator at two different time instances along with the two injections locations.

lifter within the region ($-0.05m < z < 0.05m$) where the lifter is fully submerged in the medium. To explain the aforementioned misplacement, the trajectories of PP particles within the region under examination are illustrated in Figure 12. As observed, upon their injection, some PP particles are drawn by the inlet flow and get trapped in recirculation zones both behind and beyond the inlet. These particles account for the largest amount of misplacement, as they are swept by the lifter at $t = 32s$.

To study the influence of injection location, light particles (PE in this case) are injected into two different locations which are depicted in Figure 9. Location a is at a horizontal distance of 16 cm from the inlet tube, while location b is at a horizontal distance of 28 cm. As Figure 13 illustrates, the separation efficiency at location b is larger than at location a, indicating that more light particles end up at the float outlet when they are injected further away from the inlet.

3.2.2. *Trajectories of slightly heavier particles*

Polystyrene (PS) particles have a density close to the medium density, i.e. water. Hence, the drag force is more dominant in the determination of their trajectories compared to heavier particles (such as PC). As depicted in Table 5, the model predicts that 4% of these particles are misplaced at the float outlet. To elucidate the reasons behind these misplacements, the trajectories of the PS particles on the free surface and inside the drum are depicted in Figures 14 and 15 respectively. Moreover, from the latter, it can be seen that there is some amount of PS particles that are not sinking due to the high y-velocity components in the medium at $t = 26, 5s$ and they are swept by the large x-velocity component towards the float outlet where a recirculation zone exists. This zone also contains PS particles from the previous injection (red coloured particles) as depicted in the former figure. However, as can be seen in Figure 14 from $t = 28s$ to $t = 32s$, some of the PS particles are heading towards the float outlet but the rest is recirculating towards the sides of the drum, where they can be swept by the lifter ($t = 30s$ & $t = 32s$). At $t = 33s$ the lifter exits the medium but still PS particles are present on the bottom left corner of the drum which, as is shown in Figure 15, have fallen from the lifter. Furthermore, while the lifter is immersed in the medium (Figure 15 at $t = 31s$ & $t = 33s$) it can be seen that some PS particles which are sunk halfway the depth of the medium follow the flow which flows over the lifter (also shown in Figure 8(b)) and thus are ending on the free surface as indicated in Figure 15 at $t = 36s$. To avoid these misplacements, a possible solution could be a perforated lifter, which could contribute to water being displaced through the gaps and thus the particles would not be dragged by the medium when the lifter exits the free surface or moving above the lifter when the lifter is immersed in the medium.

3.3. *Separation efficiency and wall-time comparison*

Table 5 presents a comparison of the separation efficiencies of different polymer types for both CFD-DPM and CFD-DPM-DEM (collisions included) models to experimentally derived ones. The separation efficiency for the polymer types heavier than water is computed using Equation (1) while for the polymer types lighter than water, Equation (2) is employed. Convergence in the modelled separation efficiencies was achieved through four distinct periods of particle simulations, as illustrated in Figure 16. Convergence was considered reached when the separation efficiency of the first time step in a period did not deviate by more than 2% from the maximum separation number of that period. As shown in Figure 16, three periods were required to obtain a converged separation efficiency value. As shown in Table 5, the model accurately predicts separation efficiency in the cases where the particle density significantly differs from that of the liquid.

The comparison between the numerical and experimental results for PS and ABS, both having a density of 1040 $\frac{kg}{m^3}$, shows the impact of air-bubbles attachments to the injected polymers. PS, being hydrophobic like the other injected materials except ABS, is more prone to air bubble attachments, altering its apparent density. Consequently, the experimental separation efficiency for PS is only 54%, which means that 46% of PS is misplaced in the float outlet. In contrast, ABS, being hydrophilic, experiences significantly reduced probabilities of air bubble

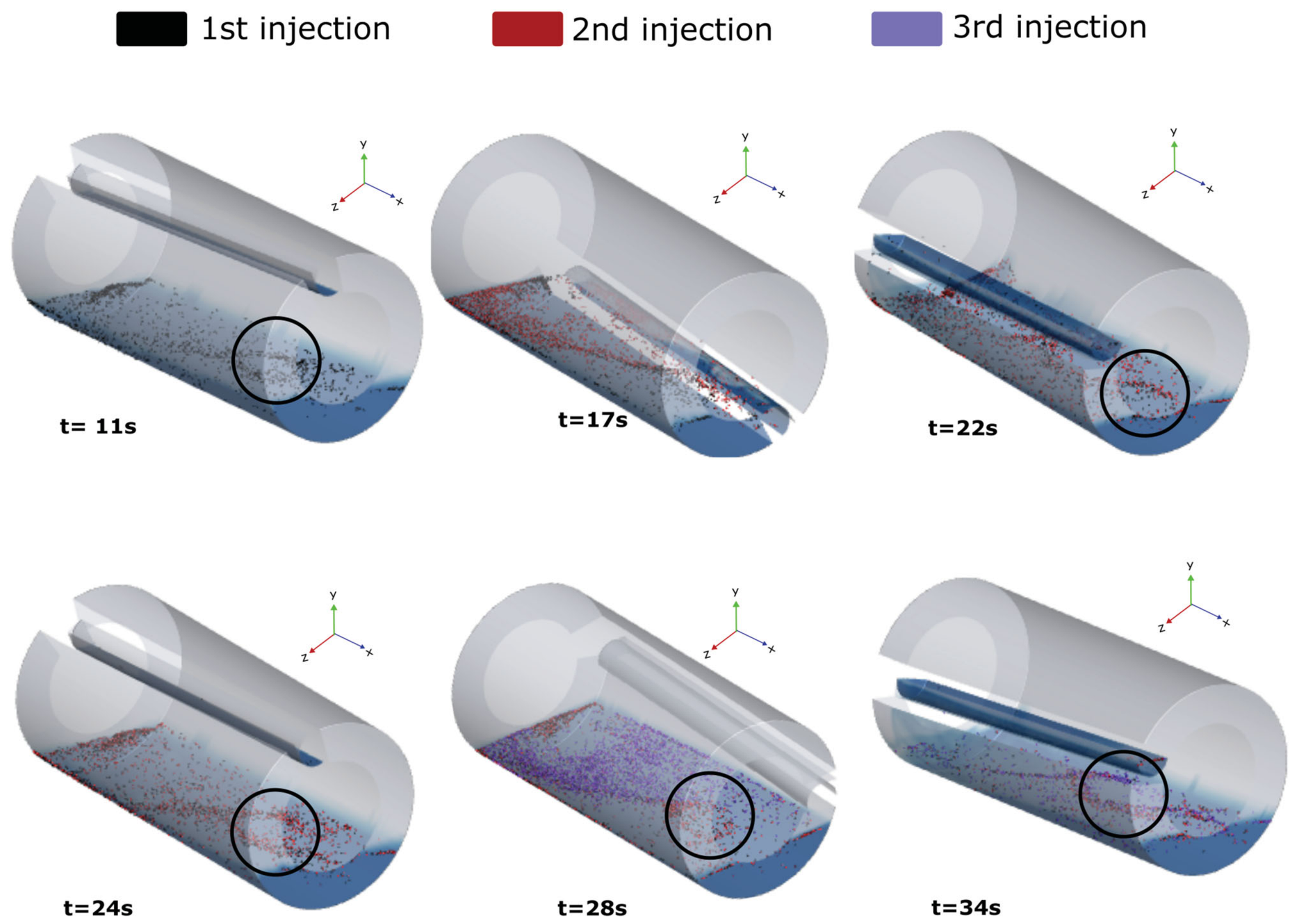

Figure 10. PP trajectories at 6 different time instances.

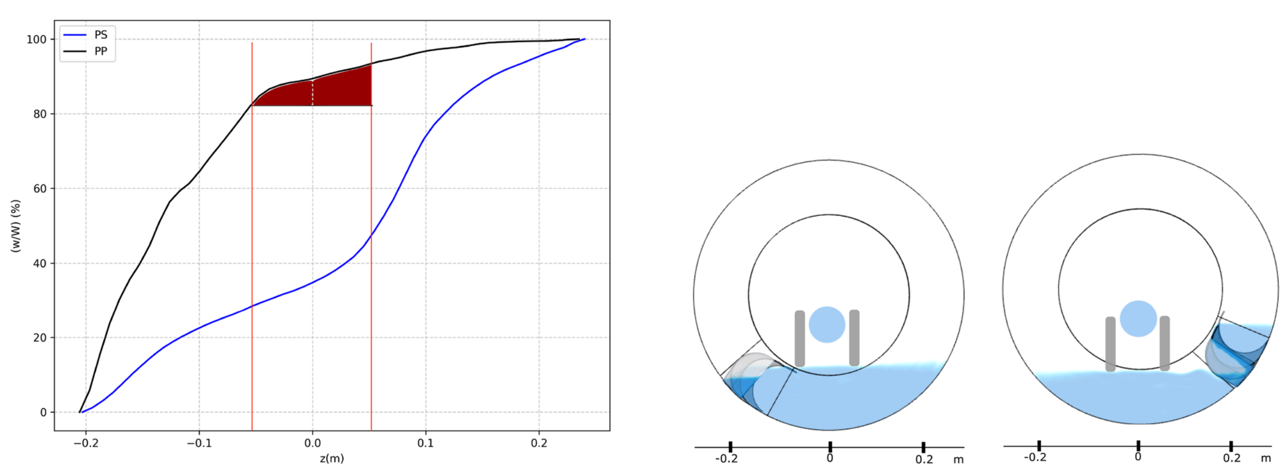

(a) Cumulative mass of PS and PP particles swept by the lifter over the width of the drum.

(b) Implementation of baffles in the drum.

Figure 11. Baffles influence on the separation of light particles.

attachments, resulting in an increased experimental separation efficiency of 77%. This efficiency, albeit improved in the experiments, still demonstrates a deviation of 17–19% from the predicted one by the model, underscoring the model's limitation in accounting for air bubble dynamics. Conversely, the predicted separation

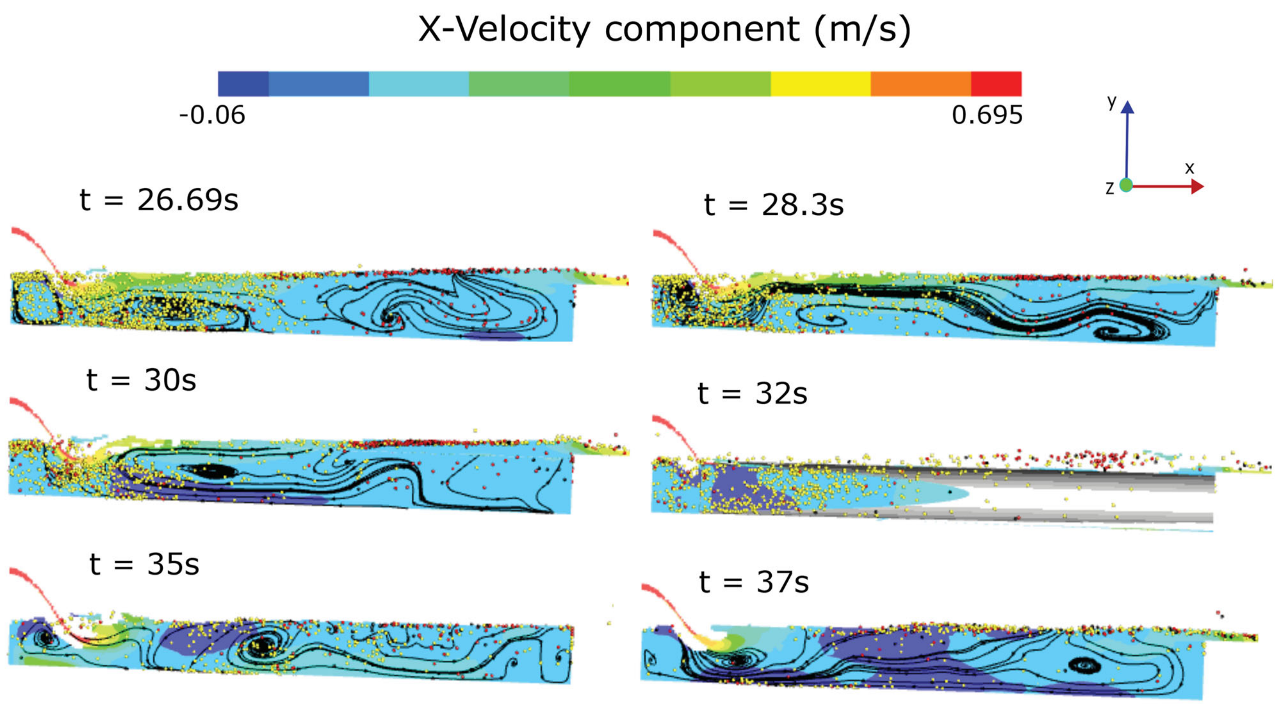

Figure 12. Trajectories of PP particles on the free surface during the third period of the drum's rotation.

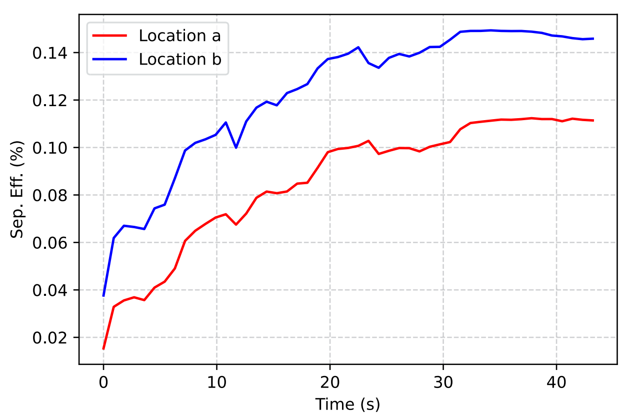

Figure 13. Separation efficiency between the two injections locations.

efficiency for the heavier PC particles deviates 3–5% from the experimental, indicating that at this density the air-bubbles attachments are not as significant as in the cases of PS and ABS. Additionally, the results of the CFD-DPM-DEM model, as included in Table 5, show no significant increase in the accuracy of the predicted separation efficiency for all types of polymer.

Figure 17 depicts the separation performance for the case of injection location *b* (see Figure 9) and curtains-baffles implementation in the drum. It is important to note that separation efficiencies were calculated using equation 1 for all polymer types. Therefore, for objects lighter than 940 kg/m^3, the misplacements are predicted to be less than 10% contrary to the case without curtains-baffles in which the misplacements were over 88%. However, misplacements of light objects increase when the polymer's density is close to the medium's density. For instance, a polymer with a density of 1000 kg/m^3 results in 55% of it ending in the sink outlet, whereas a polymer with a density of 980 kg/m^3 results in 20% ending in the sink outlet. Furthermore, heavy objects whose density is close to medium's density are not separated efficiently either, indicating a weakness of a rotating drum to separate efficiently objects whose densities are close to the medium's density.

Table 6. Wall time comparison between the two methodologies.

Time (sec)	Tested methodology	Standard methodology
Flow time solved	48	0.57
Wall-time	165600	18000

Table 6 depicts the total wall time of the simulations when using the implemented in this study methodology instead of the standard one. The latter involves solving flow equations concurrently with particle equations, while the tested methodology is detailed in Figure 5. As indicated in the table, the tested methodology reduces simulation wall time by a factor of 9. This improvement enables the simulation of 48 *sec* of flow time within 46 h. The tested methodology was executed on 16 cores with an Intel(R) Xeon(R) Gold 6248R CPU @ 3.00 GHz 2.99 GHz, while the standard methodology ran on 32 cores on the same machine.

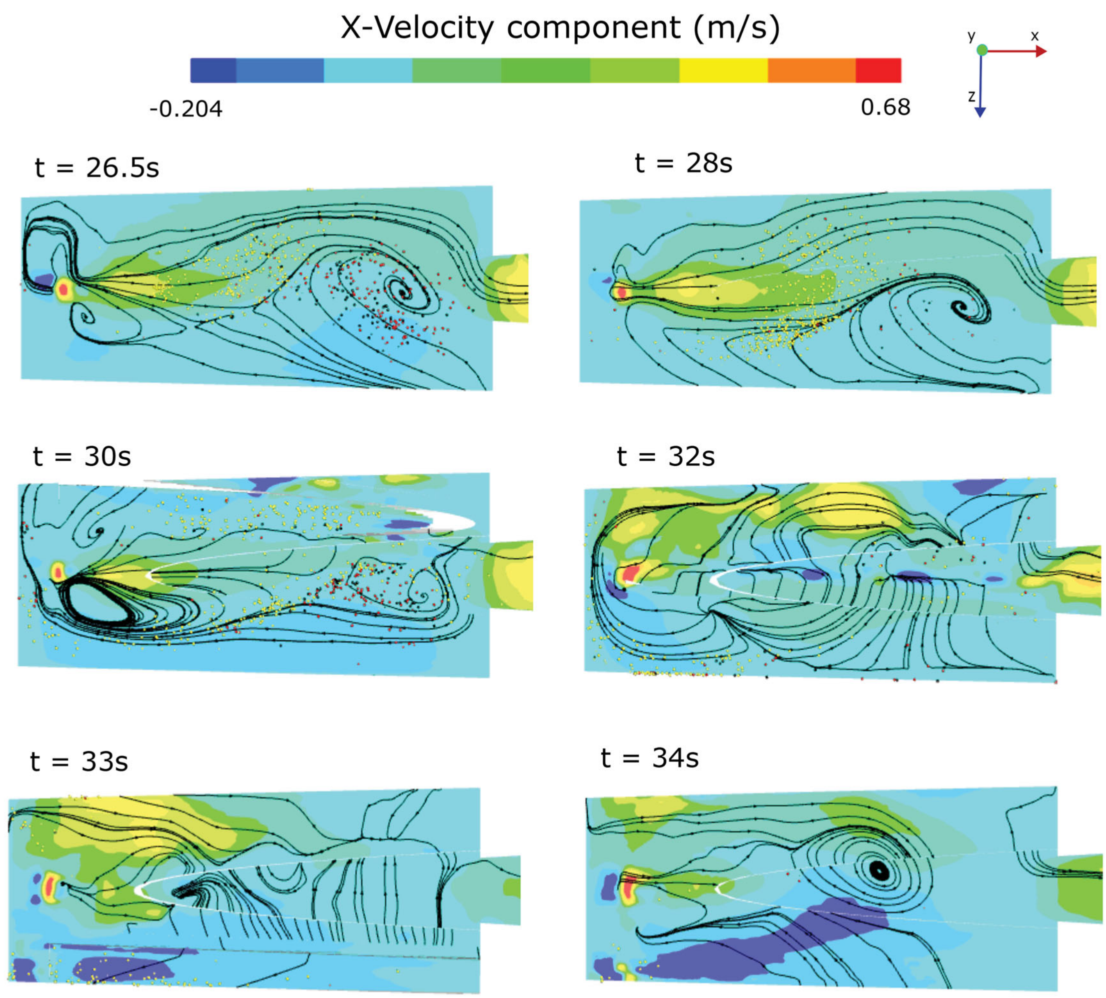

Figure 14. Trajectories of PS particles on the free surface during the third period of the drum's rotation.

4. Conclusion

Within the context of the European Strategy for plastics, the need to have plastic recyclates of equivalent mechanical properties to the virgin plastics is accentuated. This study, addresses this need, by developing a CFD model to predict the separation efficiency of a rotating drum, used to separate plastic granules. The contribution of this study is two-fold. Firstly, the introduction of a CFD model, accompanied by a simulation strategy, enables accurate tracking of dispersed plastic particles in the drum, achieving a deviation of 1–5% in separation efficiency compared to experiments. Additionally, modelling particle collisions does not enhance the accuracy of the predicted separation efficiency due to high turbulence in the flow, which makes the drag force the decisive force for the particles' trajectories. Therefore, the deviation of the predicted separation efficiency from the experimental data is mostly attributed to the errors in the turbulence modelling. The closer the particle's density to the medium's density, the larger the influence of the turbulent dispersion force and hence the error. Secondly, the study provides crucial insights into the suitability of a rotating drum for plastics separation and the impact of air bubble attachments on the separation efficiency. It demonstrates that a rotating drum is effective for separating particles with a sufficiently large density difference from the medium ($\geq$ 100 kg/m^3 for both heavy and light fractions). The interaction of lifter with the medium increases the likelihood of air bubble attachment to injected particles, influencing their hydrodynamics and, consequently, separation efficiency. This study also explores the flow pattern within the rotating drum, the influence of baffles-curtains, and the injection location's impact on the separation efficiency of floating particles. It concludes that using curtains and placing polymer injections closer to the drum's centre reduces misplacements of light polymers to 10% and 8% for densities of 940 kg/m^3 and 900 kg/m^3, respectively. Another potential modification includes a perforated lifter to avoid heavy objects falling from the lifter or heading to the free surface dragged by the displaced fluid induced by the lifter motion.

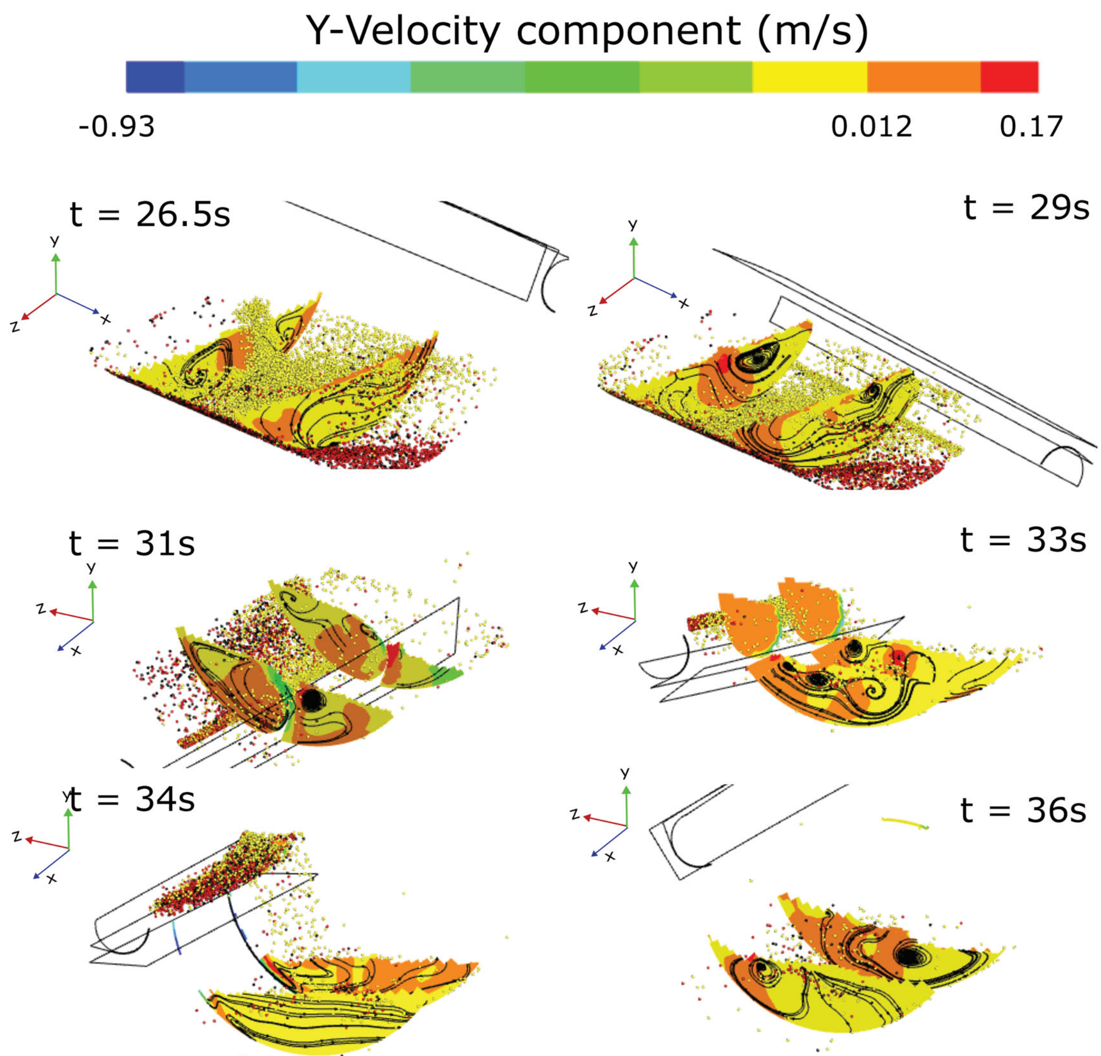

Figure 15. Trajectories of PS particles on the free surface during the third period of the drum's rotation.

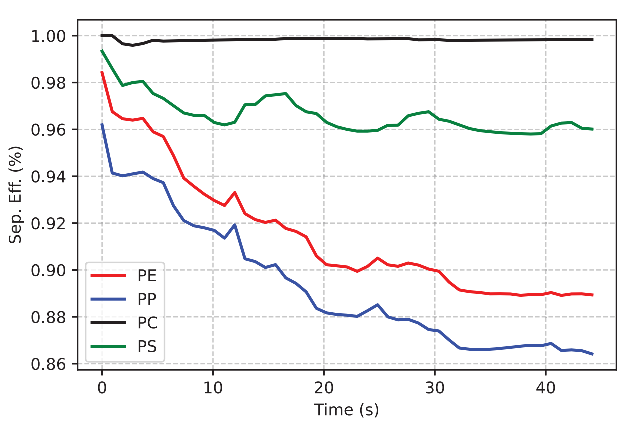

Figure 16. Convergence of separation efficiencies.

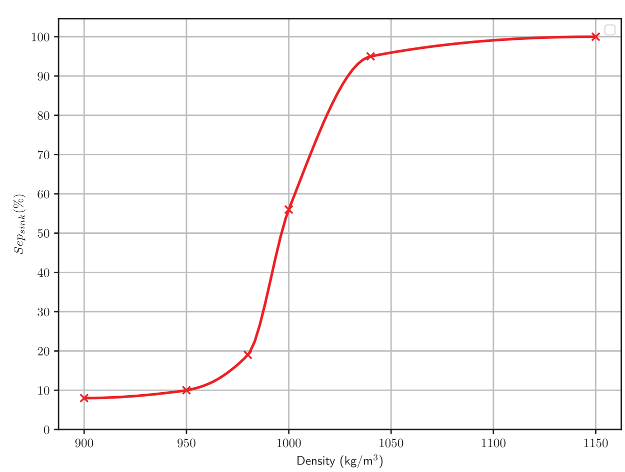

Figure 17. Separation performance of the separator when baffles-curtains are included and particles are injected from point b.

Acknowledgements

The first author would like to express his sincere gratitude to Research Foundation -Flanders (FWO) to fund this work under the project number 1S67023N. The authors also gratefully acknowledge the funding of this research by the Flanders Innovation & Entrepreneurship agency (VLAIO) through the project Plastics Recycling 4.0 (HBC.2020.2750).

Disclosure statement

No potential conflict of interest was reported by the author(s).

Data availability statement

The data that support the findings of this study are available from the corresponding author, [MV], upon reasonable request.

Funding

This work was supported by Agentschap Innoveren en Ondernemen: [Grant Number]; Fonds Wetenschappelijk Onderzoek: [Grant Number].

References

Adnan, M., Sun, J., Ahmad, N., & Wei, J. J. (2021, May). Comparative CFD modeling of a bubbling bed using a Eulerian–Eulerian two-fluid model (TFM) and a Eulerian-Lagrangian dense discrete phase model (DDPM). *Powder Technology*, *383*, 418–442. https://doi.org/10.1016/j.powtec.2021.01.063

ANSYS Inc. (2020). *Ansys Fluent, User's and Theory guide*. (Release: 2020R2).

Baguley, P. J., & Napier-Munn, T. J. (1996). A mathematical model of the dense medium drum. *Transactions of the Institute of Mining and Metallurgy Section C Mineral Processing and Extractive Metallurgy*, *105*, C1–C8.

Bakker, E. J., Rem, P. C., & Fraunholcz, N. (2009, May). Upgrading mixed polyolefin waste with magnetic density separation. *Waste Management*, *29*(5), 1712–1717. https://doi.org/10.1016/j.wasman.2008.11.006

Cundall, P. A., & Strack, O. D. L. (1979, March). A discrete numerical model for granular assemblies. *Géotechnique*, *29*(1), 47–65. Retrieved June 14, 2023, from https://www.icevirtuallibrary.com/doi/10.1680/geot.1979.29.1.47 (Publisher: ICE Publishing)

Dimas, T., Peeters, J., & Vanierschot, M. (2024). Hydrodynamic force modeling in density based plastics separation using computational fluid dynamics. In *31st annual conference of the computational fluid dynamics society of Canada csme/cfd2024* (pp. 1–6). Toronto, Ontario, Canada.

Dodbiba, G., Haruki, N., Shibayama, A., Miyazaki, T., & Fujita, T. (2002, May). Combination of sink–float separation and flotation technique for purification of shredded PET-bottle from PE or PP flakes. *International Journal of Mineral Processing*, *65*(1), 11–29. Retrieved September 15, 2021, from https://www.sciencedirect.com/science/article/pii/S0301751601000564

Eggers, A. (2020). *Modelling and optimization of high density medium drum separators* [PhD thesis]. KU Leuven. https://kuleuven.limo.libis.be/discovery/fulldisplay?docid=alma9992665201101488&context=L&vid=32KUL_KUL:KULeuven&search_scope=All_Content&tab=all_content_tab&lang=en

Eggers, A., Peeters, J. R., Waignein, L., Noppe, B., Dewulf, W., & Vanierschot, M. (2019, January). Development of a computational fluid dynamics model of an industrial scale dense medium drum separator. *Engineering Applications of Computational Fluid Mechanics*, *13*(1), 1001–1012. Retrieved August 30, 2021, from https://doi.org/10.1080/19942060.2019.1663559 (Publisher: Taylor & Francis _eprint)

European Commission. (2018). *A european strategy for plastics in a circular economy.* https://tinyurl.com/yha9kjjx.

European Commission. (2022). *Environmental impact of waste management: Revision of eu waste framework.* https://tinyurl.com/mra4dt3z.

Froelich, D., Maris, E., Haoues, N., Chemineau, L., Renard, H., Abraham, F., & Lassartesses, R. (2007, August). State of the art of plastic sorting and recycling: Feedback to vehicle design. *Minerals Engineering*, *20*(9), 902–912. Retrieved February 9, 2022, from https://www.sciencedirect.com/science/article/pii/S0892687507001392. https://doi.org/10.1016/j.mineng.2007.04.020

Gaustad, G., Olivetti, E., Kirchain, R., & Kirchain, R. (2012). Improving aluminum recycling: A survey of sorting and impurity removal technologies. *Resources, Conservation & Recycling*, *58*, 79–87. https://doi.org/10.1016/j.resconrec.2011.10.010

Gent, M. R., Menendez, M., Toraño, J., & Diego, I. (2009, March). Recycling of plastic waste by density separation: Prospects for optimization. *Waste Management & Research: The Journal for a Sustainable Circular Economy*, *27*(2), 175–187. Retrieved August 30, 2021, from https://doi.org/10.1177/0734242X08096950 (Publisher: SAGE Publications Ltd STM).

Gosman, A. D., & Loannides, E. (1983). Aspects of computer simulation of liquid-fueled combustors. *Journal of Energy*, *7*(6), 482–490. Retrieved June 13, 2023, from https://doi.org/10.2514/3.62687 (Publisher: American Institute of Aeronautics and Astronautics _eprint)

Greifzu, F., Kratzsch, C., Forgber, T., Lindner, F., & Schwarze, R. (2016, January). Assessment of particle-tracking models for dispersed particle-laden flows implemented in open foam and ansys fluent. *Engineering Applications of Computational Fluid Mechanics*, *10*(1), 30–43. Retrieved November 9, 2021, from https://www.tandfonline.com/doi/full/10.108019942060.2015.1104266

Halfi, E., Arad, A., Brenner, A., & Katoshevski, D. (2020, January). Development of an oscillation-based technology for the removal of colloidal particles from water: CFD modeling and experiments. *Engineering Applications of Computational Fluid Mechanics*, *14*(1), 622–641. Retrieved April 6, 2023, from https://doi.org/10.1080/19942060.2020.1748114 (Publisher: Taylor & Francis _eprint)

Hilton, J. E., & Cleary, P. W. (2014, September). Comparison of non-cohesive resolved and coarse grain DEM models for gas flow through particle beds. *Applied Mathematical Modelling*, *38*(17), 4197–4214. Retrieved June 14, 2023, from https://www.sciencedirect.com/science/article/pii/S0307904X14000602. https://doi.org/10.1016/j.apm.2014.02.013

Hirt, C. W., & Nichols, B. D. (1981, January). Volume of fluid (VOF) method for the dynamics of free boundaries. *Journal* *of Computational Physics*, *39*(1), 201–225. Retrieved September 7, 2021, from https://www.sciencedirect.com/science/article/pii/0021999181901455. https://doi.org/10.1016/0021-9991(81)90145-5

Hori, K., Tsunekawa, M., Ueda, M., Hiroyoshi, N., Ito, M., & Okada, H. (2009). Development of a new gravity separator for plastics —a hybrid-jig—. *Materials Transactions*, *50*(12), 2844–2847. https://doi.org/10.2320/matertrans.M-M2009825

Lu, J., Xu, J., Kumagai, S., Kameda, T., Saito, Y., & Yoshioka, T. (2019, June). Separation mechanism of polyvinyl chloride and copper components from swollen electric cables by mechanical agitation. *Waste Management*, *93*, 54–62. Retrieved December 1, 2023, from https://www.sciencedirect.com/science/article/pii/S0956053X19303241. https://doi.org/10.1016/j.wasman.2019.05.024

Markauskas, D., Kruggel-Emden, H., & Scherer, V. (2018, February). Numerical analysis of wet plastic particle separation using a coupled DEM-SPH method. *Powder Technology*, *325*, 218–227. Retrieved April 5, 2023, from https://www.sciencedirect.com/science/article/pii/S0032591017308902. https://doi.org/10.1016/j.powtec.2017.11.021

Menter, F. R. (1994, August). Two-equation eddy-viscosity turbulence models for engineering applications. *AIAA Journal*, *32*(8), 1598–1605. Retrieved April 20, 2023, from https://arc.aiaa.org/doi/10.25143.12149

Morsi, S. A., & Alexander, A. (1972). An investigation of particle trajectories in two-phase flow systems. *Journal of Fluid Mechanics*, *55*(2), 193–208. https://doi.org/10.1017/S0022112072001806

Nascimento, S. M., Lima, R. M., Brandão, R. J., Santos, D. A., Duarte, C. R., & Barrozo, M. A. S. (2022, March). Comparison between the Eulerian (CFD) and the Lagrangian (DEM) approaches in the simulation of a flighted rotary drum. *Computational Particle Mechanics*, *9*(2), 251–263. Retrieved December 1, 2023, from https://doi.org/10.1007/s40571-021-00407-z

Panchal, A., & Menon, S. (2021, August). A hybrid Eulerian-Eulerian/Eulerian-Lagrangian method for dense-to-dilute dispersed phase flows. *Journal of Computational Physics*, *439*, 110339. Retrieved December 1, 2023, from https://www.sciencedirect.com/science/article/pii/S0021999121002345. https://doi.org/10.1016/j.jcp.2021.110339

Pang, X., Wang, C., Yang, W., Fan, H., Zhong, S., Zheng, W., Zou, H., & Chen, S. (2022, December). Numerical simulation of a cyclone separator to recycle the active components of waste lithium batteries. *Engineering Applications of Computational Fluid Mechanics*, *16*(1), 937–951. Retrieved April 6, 2023, from https://doi.org/10.1080/19942060.2022.2053343 (Publisher: Taylor & Francis _eprint)

PlasticsEurope. (2022). *Plasticseurope circularity report 2022.* https://tinyurl.com/39y5myb6

Rong, W., Feng, Y., Schwarz, P., Witt, P., Li, B., Song, T., & Zhou, J. (2020, February). Numerical study of the solid flow behavior in a rotating drum based on a multiphase CFD model accounting for solid frictional viscosity and wall friction. *Powder Technology*, *361*, 87–98. Retrieved April 5, 2023, from https://www.sciencedirect.com/science/article/pii/S0032591019308307. https://doi.org/10.1016/j.powtec.2019.10.034

Rousseau, M., & Melin, A. (1989, February). The processing of non-magnetic fractions from shredded automobile scrap: A review. *Resources, Conservation and Recycling*, *2*(2), 139–159. Retrieved March 31, 2023, from https://www.sciencedirect.com/science/article/pii/0921344989900219. https://doi.org/10.1016/0921-3449(89)90021-9

Santos, D. A., Petri, I. J., Duarte, C. R., & Barrozo, M. A. S. (2013, December). Experimental and CFD study of the hydrodynamic behavior in a rotating drum. *Powder Technology*, *250*, 52–62. Retrieved April 5, 2023, from https://www.sciencedirect.com/science/article/pii/S0032591013006062. https://doi.org/10.1016/j.powtec.2013.10.003

Serranti, S., Luciani, V., Bonifazi, G., Hu, B., & Rem, P. C. (2015, January). An innovative recycling process to obtain pure polyethylene and polypropylene from household waste. *Waste Management*, *35*, 12–20. Retrieved January 25, 2022, from https://www.sciencedirect.com/science/article/pii/S0956053X14005017. https://doi.org/10.1016/j.wasman.2014.10.017

Tajfirooz, S., Meijer, J., Dellaert, R., Meulenbroek, A., Zeegers, J., & Kuerten, J. (2021). Direct numerical simulation of magneto-archimedes separation of spherical particles. *Journal of Fluid Mechanics*, *910*, A52. https://doi.org/10.1017/jfm.2020.1001

Tierean, M. H., Rem, P. C., Maio, F. D., Hu, B., Houzeaux, G., & Baltes, L. S. (2012). Magnetic fluid equipment for sorting secondary polyolefins from waste. *Environmental Engineering and Management Journal*, *12*(5), 951–958. https://doi.org/10.30638/eemj.2013.118

Xia, Y., & Peng, F. F. (2007, January). Effect of structured plates on fine coal gravity separation in a liquid fluidized bed system. *Engineering Applications of Computational Fluid Mechanics*, *1*(3), 164–180. Retrieved April 6, 2023, from https://doi.org/10.1080/19942060.2007.11015190 (Publisher: Taylor & Francis _eprint)

Yayla, S., Ibrahim, S. S., & Olcay, A. B. (2017, January). Numerical investigation of coalescing plate system to understand the separation of water and oil in water treatment plant of petroleum industry. *Engineering Applications of Computational Fluid Mechanics*, *11*(1), 184–192. Retrieved April 6, 2023, from https://doi.org/10.1080/19942060.2016.1273137 (Publisher: Taylor & Francis _eprint)

Yuan, H., Fu, S., Tan, W., He, J., & Wu, K. (2015). Study on the hydrocyclonic separation of waste plastics with different density. *Waste Management*, *45*, 108–111. https://www.sciencedirect.com/science/article/pii/S0956053X15000768 (Urban Mining). https://doi.org/10.1016/j.wasman.2015.01.037

Yuan, J., Li, H., Qi, X., Hu, T., Bai, M., & Wang, Y. (2020, January). Optimization of airflow cylinder sieve for threshed rice separation using CFD-DEM. *Engineering Applications of Computational Fluid Mechanics*, *14*(1), 871–881. Retrieved April 6, 2023, from https://doi.org/10.1080/19942060.2020.1778540 (Publisher: Taylor & Francis _eprint)

Zhu, M., Hu, D., Xu, Y., & Zhao, S. (2020). Design and computational fluid dynamics analysis of a three-phase decanter centrifuge for oil-water-solid separation. *Chemical Engineering & Technology*, *43*(5), 1005–1015. Retrieved April 5, 2023, from https://onlinelibrary.wiley.com/doi/abs/10.1002ceat.201900245 (_eprint)